Available online at www.sciencedirect.com
ScienceDirect
Trans. Nonferrous Met. Soc. China 34(2024) 3963−3977
Transactions of Nonferrous Metals Society of China
www.tnmsc.cn

Effects of nanostructuring on mechanical and tribological behaviors of FeCoNi medium-entropy alloy

Yan CHEN[1], Heng LI[2], Si-en LI[1], Gui-xun SUN[1], Liang ZHAO[1], Chao-quan HU[1,3], Wei ZHANG[4], Guo-dong TONG[4], Xue-gang CHEN[4], Shuang HAN[1], Hong-xiang ZONG[2], Jun LI[4], Jian-she LIAN[1]

1. Key Laboratory of Automobile Materials, Ministry of Education, College of Materials Science and Engineering, Jilin University, Changchun 130025, China;
2. State Key Laboratory for Mechanical Behavior of Materials, Xi'an Jiaotong University, Xi'an 710049, China;
3. State Key Laboratory of Superhard Materials, Jilin University, Changchun 130025, China;
4. China FAW Corporation Limited, Changchun 130011, China

Received 16 April 2023; accepted 7 November 2023

Abstract: The effects of nanostructuring on the mechanical and dry-sliding wear behaviors of a FeCoNi medium-entropy alloy (MEA) were systematically investigated through nano-indentation and ball-on-disc wear tests. The results show that reducing the grain size down into the nano-meter regime, on the one hand, significantly elevates the hardness of the FeCoNi alloy, and on the other hand, facilitates the formation of a surface oxide layer. As a result, the wear rate of the nanocrystalline (NC) FeCoNi alloy is one order of magnitude lower than its coarse-grained counterpart. The NC FeCoNi alloy also exhibits obviously enhanced wear resistance compared with conventional NC Ni and Ni-based alloys in terms of both lower wear rate and friction coefficient. Such enhancement in tribological properties mainly stems from the improved strain hardening ability, owing to the inevitable concentration heterogeneity in MEA that imposes extra resistance to dislocation motion.

Key words: medium-entropy alloy; FeCoNi alloy; nanocrystalline; mechanical behavior; dry-sliding wear; concentration undulation

1 Introduction

In recent years, multi-principal element alloys, typified by medium entropy alloys (MEAs) for ternary systems and high entropy alloys (HEAs) for quinary or senary systems, have attracted much attention. This is mainly because, on the one hand, they represent an innovative strategy of alloy design that focuses on the unexplored central regions of multi-element phase diagrams [1], and on the other hand, they exhibit unique combinations of mechanical and physical properties [2]. In particular, exceptional ductility and fracture toughness at cryogenic temperatures have been discovered for the HEAs/MEAs with face-centered cubic (FCC) structures [3]. These single-phase alloys have also been reported to be more resistant to radiation damage [4]. These factors make FCC HEAs/MEAs potential candidates for the new generation of high-performance structural materials. However, the yield strength of FCC HEAs/MEAs is generally not sufficiently high at room temperature, which severely restricts their applications [5]. Thus, various strengthening strategies have been utilized to enhance the strength of FCC HEAs/MEAs, such

Corresponding author: Heng LI, Tel: +86-29-82668614, E-mail: liheng16@xjtu.edu.cn;
Shuang HAN, Tel: +86-341-85094375, E-mail: shuanghan@jlu.edu.cn
DOI: 10.1016/S1003-6326(24)66651-3

as manipulating hierarchical microstructures [6], controlling phase stability [7] and introducing second phase particles [8].

Nanostructuring has also been proved to be an effective way to improve the strength of FCC MEAs/HEAs [9]. By refining grains down to nano-scale or introducing nano-twins, the yield strength and hardness of MEAs/HEAs can be substantially elevated, as a large volume of grain boundaries (GBs) and twin boundaries (TBs) can act as barriers to obstruct dislocation motion [10,11]. In addition to the stress−strain response, the friction and wear properties of MEAs/HEAs are also key factors affecting the safety, reliability and lifetime of metallic materials for their applications in harsh environments [12]. In particular, nanostructured HEAs/MEAs are always present in the form of coatings or films due to preparation methods such as magnetron sputtering [10,13], electrode-position [14] and laser cladding [15,16]. Thus, for nanostructured MEAs/HEAs, it is very important to study their tribological properties. For conventional nanocrystalline (NC) metals and alloys, clear correspondences between the reduced wear rate and nanostructuring have always been observed [17,18]. More than that, the microstructures of NC MEAs/HEAs are much more complex than those of conventional NC metals and dilute solid solutions [19]. The heterogeneities come from the multiple constituent species, including clusters of solute atoms with local chemical order [20] and their complexes [21,22], together with the high density of defects from the NC structure, should substantially affect not only the mechanical but also the tribological properties of these NC MEAs/HEAs. Thus, a lucid understanding of the composition–structure–property relationships in such a unique structural-compositional space is of critical important for rational designing of NC MEAs/HEAs with appropriate structural robustness.

In the present study, the effects of nano-structuring on the friction and wear properties of MEAs/HEAs were systematically investigated. We selected an equiatomic FeCoNi alloy as our model system. The reasons are threefold: (1) FeCoNi is an important variant of Cantor alloy (FeMnCrCoNi) that stands out as the most successful HEA due to its outstanding mechanical properties and can bridge the gap between traditional solid solutions and MEAs/HEAs [23]; (2) FeCoNi is a desirable base alloy for microstructural manipulation for superior mechanical properties [24]; (3) The excellent magnetic properties of FeCoNi alloys endow them with great industrial potential [25,26]. More than that, HEAs/MEAs consisting of 3d transition metal class elements (such as Fe, Co and Ni) are easy of electrochemical co-deposition from the modified Watts-type bath [27]. Electrodeposition has been widely used in synthesizing NC metals and alloys, as it exhibits significant advantages over other methods for preparing NC materials, including wide applicability, flexibility in size and shape, and high potential for industrial applications [28]. Thus, electrodeposition was utilized here to fabricate the NC FeCoNi model materials. The mechanical behaviors and tribological properties of the NC alloys were explored by performing ball-on-disc dry sliding wear tests with varying loads and sliding velocities, and then were compared with those of their coarse-grained (CG) counterparts and conventional NC metals. The underlying deformation and wear mechanisms of NC and CG FeCoNi alloys were also discussed in detail.

2 Experimental

The NC FeCoNi alloys were prepared by pulsed electrodeposition with a modified Watts-type bath containing nickel sulfate, cobalt sulfate and ferrous sulfate. Saccharin and 1, 4-butynediol were supplied as grain refining agent and stress reliever, respectively. With the action of saccharin, complex compounds formed on the surface of cathode and then decreased the diffusion rate of adsorbed metal ions. As a result, the frequency of nucleation sites increased, which promoted grain refinement to nanoscale [29]. A high purity Ni sheet (200 mm × 100 mm × 3 mm) and a low carbon steel sheet (100 mm × 100 mm × 2 mm) were used as the anode and cathode, respectively. The deposition was started with a peak current density of 20 A/dm^2. During the deposition process, an average current density of 2.0 A/dm^2 was used, while the pH and the bath temperature were maintained at (2.5±0.2) and (55±2) °C, respectively. The thickness of the resultant NC FeCoNi sample is ~400 μm. The commercial FeCoNi alloys with equiatomic composition (Fe33.95Co33.16Ni32.89, in at.%), prepared by vacuum melting, were purchased from ONA Target Corporation in the as-cast condition.

The compositions of the NC and CG FeCoNi alloys were examined using a scanning electron microscope (SEM, VEGA3-TESCAN) equipped with an energy-dispersive X-ray spectrometer (EDS). The phase structure of the NC FeCoNi alloy was detected by X-ray diffraction (XRD, Rigaku D/MAX 2500PC). Transmission electron microscopy (TEM, JEM−2100F) characterizations were performed for the detailed microstructure of the NC FeCoNi alloy. The TEM samples were first thinned manually to a thickness of 30−50 μm, then electropolished and eventually made electron-transparent by ion-milling. The backscattered electron image (BSE) of CG FeCoNi was obtained by a field emission SEM (FESEM, JSM−7900F) equipped with an Oxford Instruments BSE detector.

Nanoindentation tests were performed on a Nanoindentation G200 nanoindenter with a Berkovich diamond indenter at room temperature. Before nanoindentation tests, all specimens were polished to a mirror-like finish surface. The indentation hardness was measured using a continuous stiffness measurement method (CSM) at an input strain rate of 0.04 s^{-1}. The rate sensitivity was investigated via strain rate jump tests (SRJ). Four different strain rates (0.3, 0.045, 0.007 and 0.001 s^{-1}), changing for every 250 nm depth, were used in a single indentation test. The indenter was unloaded to 10% of the maximum load and held for 100 s for thermal drift correction, and the indentation under the same conditions was repeated at least 10 times. The tribological behavior was tested on a CSM ball-on-dis tribometer at room temperature under dry sliding conditions. The NC and CG FeCoNi samples were cut into discs with a diameter of 5 mm and a thickness of approximately 400 μm. The sliding surface of the sample was polished to a roughness of 0.40 μm (R_a). The counterface ball with a diameter of 3 mm was made of Al_2O_3. Before testing, the sliding radius was set as 1.5 mm. The wear tests were performed at a normal load of 5 N and constant sliding speeds of 3.5, 5 and 7 cm/s, each for 5000 sliding cycles. The wear rate was calculated as the volume loss divided by the sliding distance. The volume loss was measured by a 3-D surface profilometer. For each sliding speed, at least three samples were tested and the final values of the coefficient of friction (COF) and wear rate were quoted for the average of multiple measurements.

3 Results

3.1 Microstructure

The SEM−EDS results reveal that the compositions of both the NC and CG alloys are nearly equiatomic (Table 1). Figure 1 shows the XRD patterns of the NC FeCoNi alloy, from which all the diffraction peaks can be indexed as a single FCC structure without any secondary phase. The microstructure of the NC sample was further characterized by TEM, as shown in Fig. 2. The NC FeCoNi alloy consisted of equiaxed grains with a narrow distribution from 5 to 35 nm and a mean grain size of ~26 nm. The selected area diffraction (SAD) pattern confirms a single-phase FCC structure (inset in Fig. 2(a)), which is consistent with the XRD result. The addition of Fe elevates the stacking fault energy of the NC alloy, so only sporadic growth twins can be detected in the as-deposited samples. Statistical high resolution transmission electron microscopy (HRTEM) examinations reveal that nano-sized twins can only be found in 5% of the grains, and the average twin thickness is ~13 nm (Fig. 2(c)). Figure 2(d) displays a typical BSE image of the CG FeCoNi alloy. The average grain size of the CG alloy is ~784 μm.

Table 1 Compositions of NC and CG FeCoNi alloys (at.%)

Specimen	Fe	Co	Ni
NC	34.2	33.1	32.7
CG	33.4	33.3	33.3

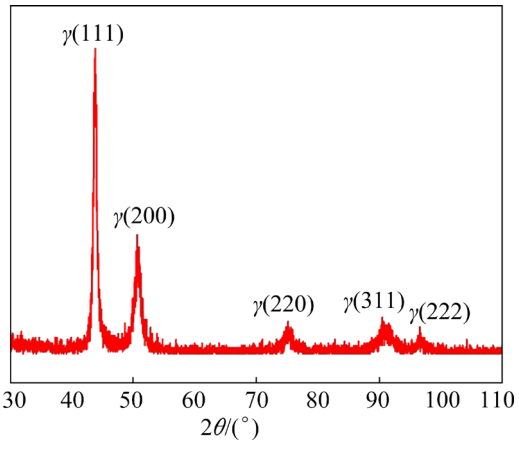

Fig. 1 XRD pattern of NC FeCoNi alloy

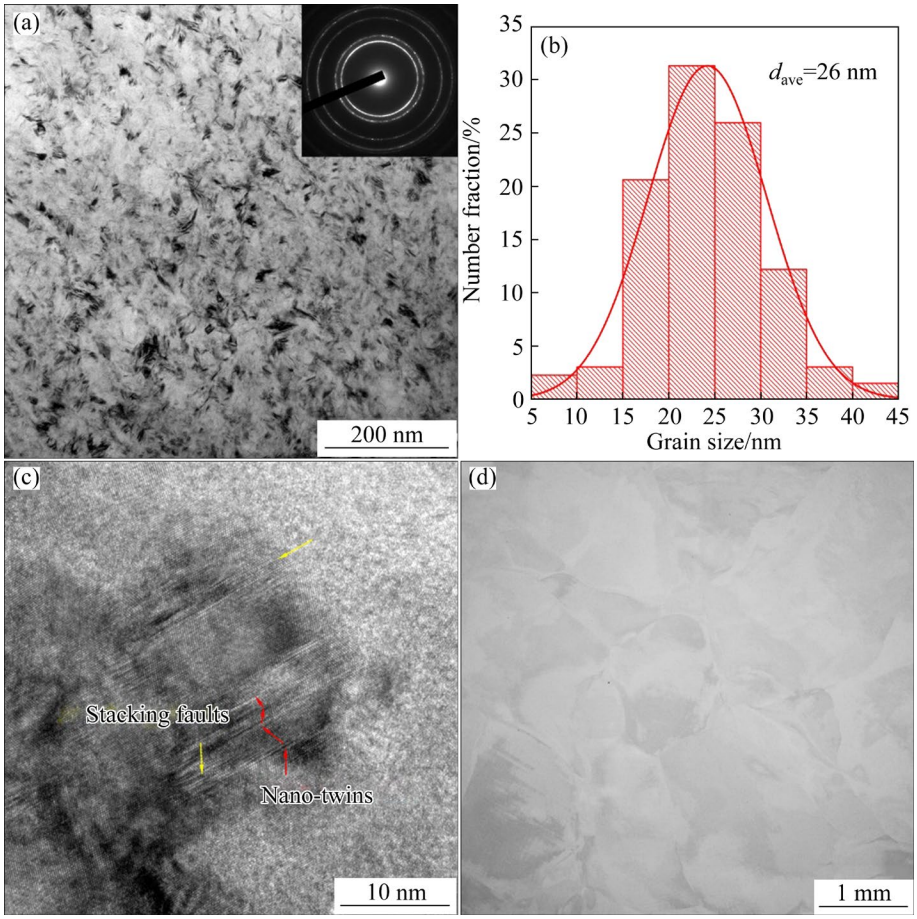

Fig. 2 (a) Bright field TEM image of NC FeCoNi alloy; (b) Corresponding statistical grain size distribution; (c) HRTEM image of nano-twins and stacking faults in grain interiors of NC FeCoNi alloy; (d) Typical BSE image of CG FeCoNi alloy

3.2 Nano-mechanical properties

The load−displacement (H–P) curves and the corresponding hardness versus displacement curves are given in Fig. 3. Figure 3(b) shows the plots of the hardness versus the depth of indentation, which were obtained using CSM unit continuously during indentation for the NC and CG FeCoNi alloys, respectively. The NC FeCoNi alloy exhibits a hardness of ~5.8 GPa, much higher than that of the CG one (2.0 GPa). The modulus of the two alloys, also determined by nano-indentation, is ~160 GPa.

The strain rate sensitivity of flow stress (m) and the apparent activation volume (V*) were estimated based on the indentation results to explore the underlying deformation mechanisms. The value of m is defined as

$$m=\frac{\partial \ln H}{\partial \ln \dot{\varepsilon}} \tag{1}$$

where H and $\dot{\varepsilon}$ are the hardness and the strain rate, respectively. The V* is related to the m, which is defined as

$$V^{*}=3\sqrt{3}kT\frac{\partial \ln \dot{\varepsilon}}{\partial H} \tag{2}$$

where k is the Boltzmann constant (1.38×10^{-23} J/K), T is thermodynamic temperature, and $\dot{\varepsilon}$ and H are the strain rate and hardness, respectively. The fitting curves of m and V^{*} are shown in Figs. 3(c) and (d) for the NC and CG FeCoNi alloys, respectively. The values of m and V* for NC FeCoNi were calculated to be 0.0292 and $7.02b^3$, while they are 0.0246 and $24.18b^3$ for CG FeCoNi.

3.3 Friction and wear properties

3.3.1 COF and wear rate

The COF, defined as the ratio of tangential force and normal force, was measured as a function of sliding cycles for different sliding speeds. Figures 4(a) and (b) show the variations of COF with sliding cycles for NC and CG FeCoNi alloy, respectively. After hundreds of cycles, the COFs for

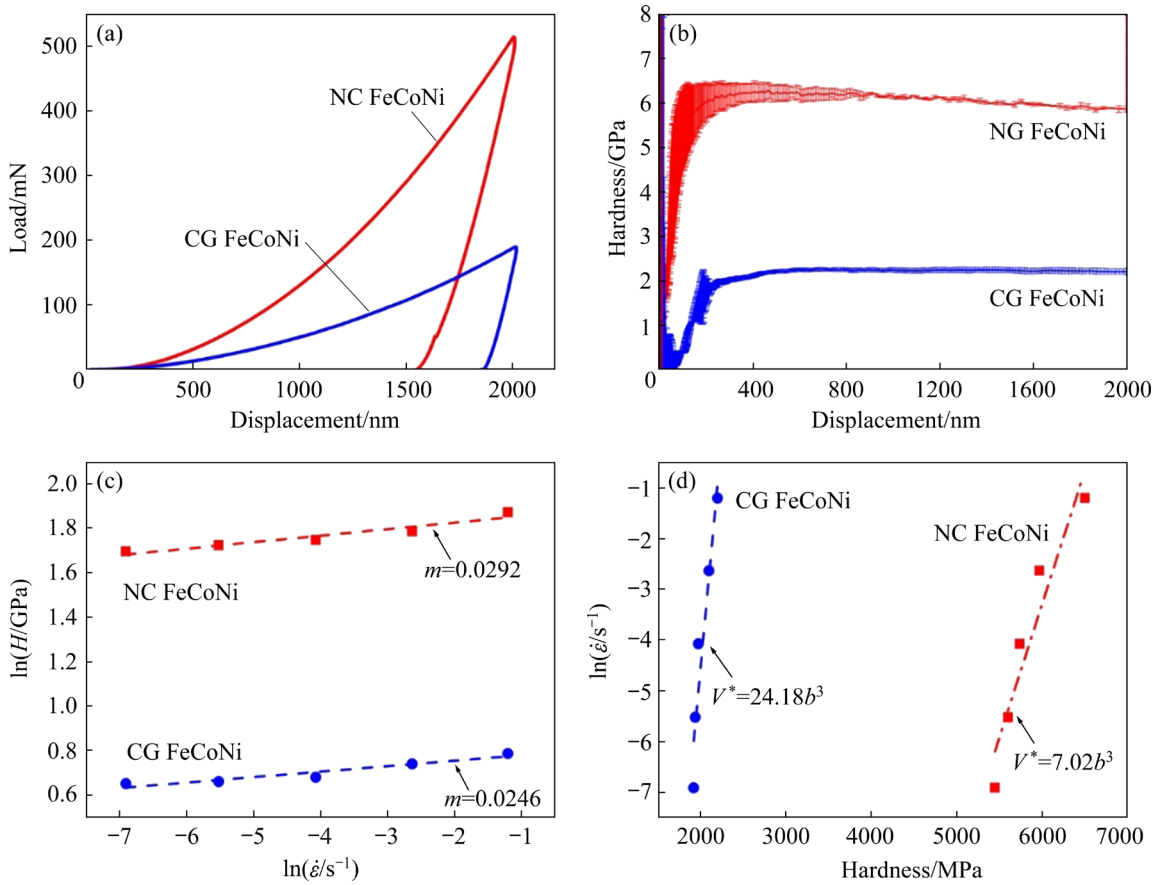

Fig. 3 Load−displacement curves (a), hardness variations (b), logarithmic plots of hardness as function of indentation strain rate $\dot{\varepsilon}$ (c), and plots of $\ln\dot{\varepsilon}$ versus hardness (d) for NC and CG FeCoNi alloys

both alloys become stable. The COF of NC FeCoNi alloy was approximately 0.470, 0.515 and 0.528 for different sliding speeds of 3.5, 5 and 7 cm/s, respectively. While for CG FeCoNi alloy, the COF was 0.495, 0.537 and 0.545. As shown in Fig. 4(c), the variations of COF for both NC and CG FeCoNi alloys exhibit the similar trends: (1) with the increasing sliding speed, the COF increases for both alloys; (2) at the same sliding speed, the COF of NC FeCoNi alloy is slightly lower than that of the CG alloy. The wear rate, W, is another key factor to evaluate the wear properties of specific materials. It can be calculated as

$$W=\frac{1}{2\pi R}\frac{\Delta V}{\Delta NL} \tag{3}$$

where R is the radius, ΔV is volume loss ($\Delta V=\Delta S\times 2\pi R$, ΔS is the cross-sectional area of wear track, which was measured by 3-D surface profilometer), ΔN is the sliding cycles, and L is the applied normal load. The W of the NC FeCoNi alloy was calculated to be 0.925×10^{-5}, 1.288×10^{-5} and 2.455×10^{-5} mm³/N·m for sliding speeds of 3.5, 5 and 7 cm/s, respectively. While for the CG alloy the values are 21.2×10^{-5}, 24.8×10^{-5} and 32×10^{-5} mm³/(N·m). At the same sliding speed, the wear rate of CG FeCoNi alloy is significantly higher than that of NC FeCoNi alloy, while for both alloys the W increased with increasing sliding speed (Fig. 4(d)).

3.3.2 Contact surface morphologies

The morphologies of worn surface for the NC and CG FeCoNi alloys were examined by SEM, as shown in Fig. 5. For both alloys, delamination wear and abrasive wear prevail for all sliding speeds, regardless of the grain size. The former was characterized by the formation of delaminated crater (indicated by the yellow arrows) while the later was characterized by fine grooves parallel to the sliding direction (indicated by red arrows) [30]. But for the NC specimen, as the sliding speed increases to 7 cm/s, continuous distribution of small voids can be observed on the worn surface (Fig. 5(e), marked by the blue arrows), indicating the occurrence of adhesive wear.

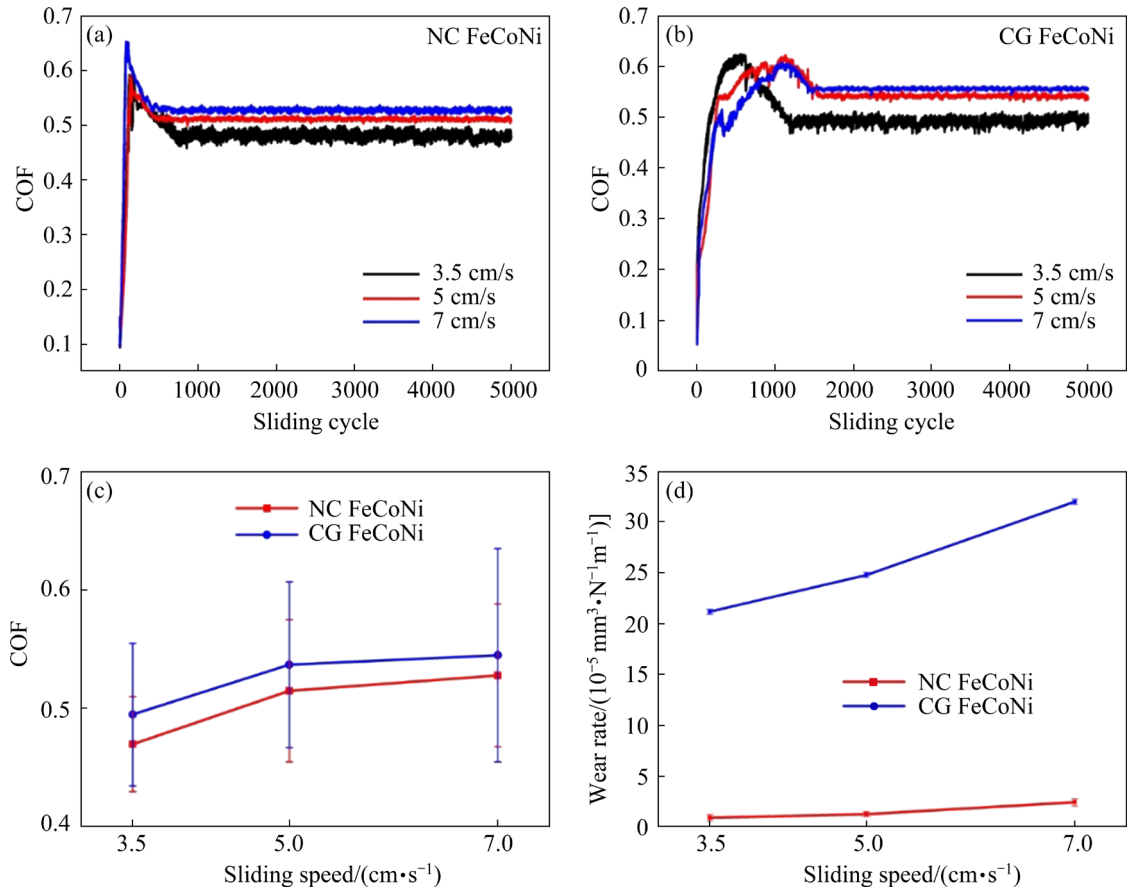

Fig. 4 Variations in COFs for NC (a) and CG (b) FeCoNi alloys, and average COFs (c) and wear rates (d) of NC and CG FeCoNi alloys at different sliding speeds

The wear tracks were further characterized by laser scanning confocal microscopy (LSCM). Figure 6 displays the three-dimensional (3-D) wear track profiles obtained in both NC and CG FeCoNi samples after sliding wear with 5000 cycles at various sliding speeds (3.5, 5 and 7 cm/s) but a fixed load (5 N). It is visible that for the NC FeCoNi alloy, both the width and the depth of the wear tracks increase with sliding speed. But for the CG FeCoNi, the width of the wear tracks remained almost constant over the whole speed range, while the depth of the wear track increased obviously. For a given sliding speed, NC FeCoNi generally has relatively narrower and shallower wear track than its CG counterpart, as clearly illustrated by different colors in the 3-D profiles.

According to the 3-D surface profiles of the wear tracks provided in Fig. 6, plastic deformation proceeded during the sliding wear of both alloys. This is not surprising due to the relatively high applied normal load. The contact Hertzian stress (σ_H) on the surface can be estimated as [31]

$$\sigma_H = 0.918\sqrt[3]{\frac{P}{D^2C^2}} \tag{4}$$

where P=5 N is the normal load, D=3.125 mm is the counterface ball diameter, and C is the effective elastic modulus defined as

$$C=\left(\frac{1-\upsilon_1^2}{E_1}\right)+\left(\frac{1-\upsilon_2^2}{E_2}\right) \tag{5}$$

where E_1 and E_2 are the elastic modulus for specimen and counter-face ball, respectively, while υ_1 and υ_2 are the Poisson's ratio of the specimen and counter-face ball, respectively. The Poisson's ratio is approximately 0.3 for both specimens. The elastic modulus and Poisson's ratio of Al_2O_3 are 385 GPa and 0.26, respectively. According to Eqs. (4) and (5), the initial contact stress was calculated to be 1.65 GPa. The yield strengths of the NC and CG FeCoNi alloys were estimated from the indentation hardness to be 1.76 and 0.66 GPa, respectively. So, this initial contact stress is lower than the yield

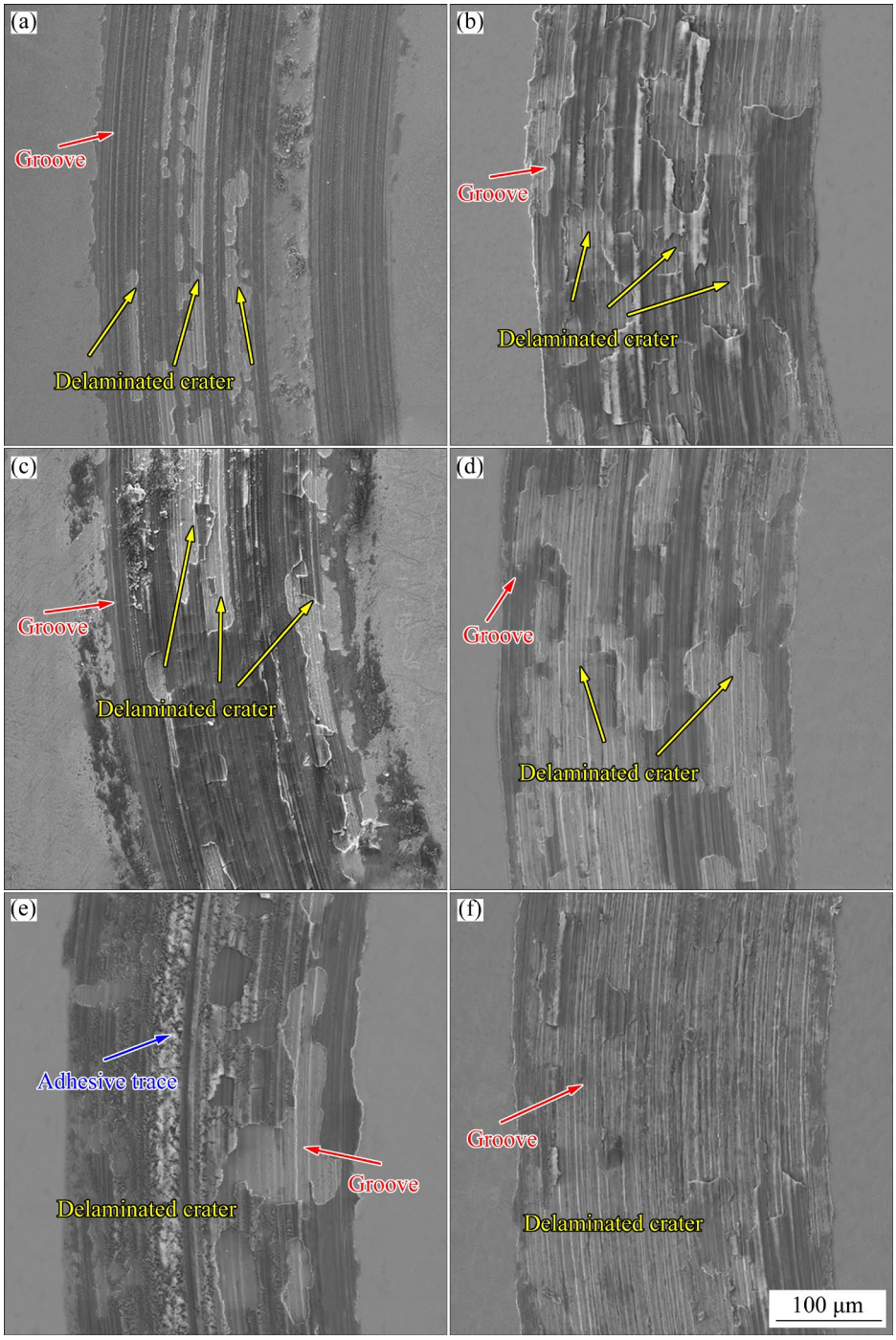

Fig. 5 SEM images of worn surfaces of NC (a, c, e) and CG (b, d, f) FeCoNi alloys at different sliding speeds: (a, b) 3.5 cm/s; (c, d) 5 cm/s; (e, f) 7 cm/s

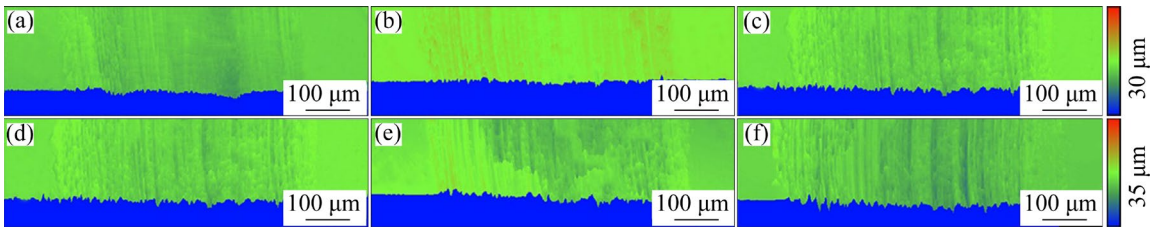

Fig. 6 3-D surface profiles of wear tracks in NC (a−c) and CG (d−f) FeCoNi alloys at different sliding speeds: (a, d) 3.5 cm/s; (b, e) 5cm/s; (c, f) 7cm/s

strength of the NC alloy but significantly higher than that of the CG one. As a result, the plastic deformation of the CG FeCoNi was first triggered by the initial stress and then proceed during sliding wear, while the plastic deformation of the NC coating was gradually involved during the dry sliding process. This is partly responsible for the different features of the wear tracks in these two alloys.

4 Discussion

4.1 Deformation mechanisms

The deformation mechanisms of both CG and NC FeCoNi alloys were analyzed based on the activation volumes (V^*) obtained during nano-indentation tests. For traditional CG FCC metals, plastic flow was achieved via intragranular dislocation interactions, i.e., cutting forest dislocations, resulting in activation volumes on the order of 100−1000b^3 [32]. However, the V^* was measured to be only ~25b^3 for the CG FeCoNi alloy in our present study. In such a case, if the dislocation interaction was still the rate-controlling mechanism, a dislocation density as high as 10^{17}−10^{18}/m^2 is needed. Such a value exceeds by far that attained in heavily cold-rolled metals (up to ~10^{16}/m^2) [33]. In fact, dynamic recovery would take place long before such high dislocation densities can be achieved. This means that there exist other rate-controlling mechanisms that mediate the plastic deformation in the CG FeCoNi alloy. It was found that the new tell-tale feature that distinguishes these HEAs/MEAs from traditional dilute solid solutions is the presence of atomic and nanometer level chemical heterogeneities such as short range order (SRO) clusters [34]. Our first-principle calculations reveal that Fe−Ni and Fe−Co ordering tend to develop in the FeCoNi alloy (Fig. 7), indicating the presence of SRO. In HEAs/MEAs, the SRO clusters raise the activation barriers and increase the lattice friction to dislocation motion [35]. As a result, dislocations move via nanoscale segment detrapping. Such nano-scale thermal activation activities always generate V^* values on the order of tens of b^3. In fact, the reported V^* values for FCC HEAs/MEAs, such as FeMnCrCoNi, FeMnCrCo and CrCoNi [36−38], are all on the same order of magnitude to the values obtained in our present CG FeCoNi alloy. Therefore, it is reasonable to conclude that the plastic deformation of the CG FeCoNi alloy was dominated by the interaction between dislocations and SRO clusters.

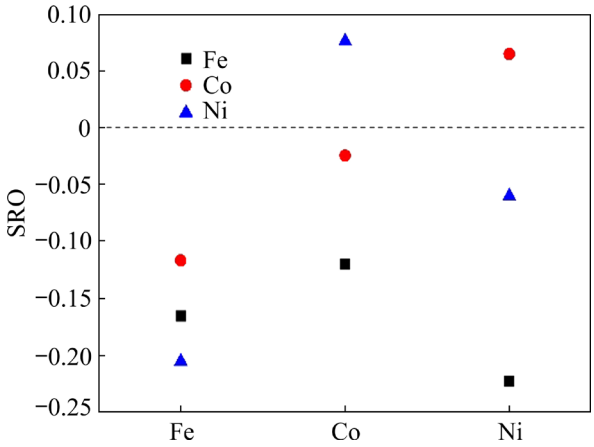

Fig. 7 Pairwise chemical short-range order (SRO) parameter in FeCoNi alloy

For NC metals, if grain boundary (GB) sliding and diffusion were the main deformation mechanisms, the expected V^* would be on the order of atomic volume, i.e., 1b^3 [39], which is much smaller than the value we measured in the NC FeCoNi alloy. Therefore, the GB-dominated deformation mechanisms can be ruled out. Moreover, pushing dislocations through high bundles of dislocations at GBs can also lead to a small V^* of several b^3, as the case in NC metals that experience severe plastic deformation. However, this is obviously not the scenario in our present study, as both the grain interior and the regions near GBs are almost clean of dislocations for electrodeposited metals [40]. Therefore, in the NC FeCoNi alloy, the activation volume of approximately 10b^3 mainly arises from the interactions between dislocations and GBs, such as dislocation emission and absorption from GBs, as well as dynamic recovery of dislocations that reside along GBs [40]. It is also worth noting that SRO clusters also exist inside the nano-grains for the present NC FeCoNi, whose interactions with dislocation may produce even smaller activation volumes than those of conventional NC metals and alloys. Based on the above analysis, it is reasonable to infer that for the NC FeCoNi alloy, the plastic deformation is mainly controlled by the interactions of dislocations with either GBs or SRO clusters.

4.2 Strengthening mechanisms

For NC metals and alloys, the relationship between the hardness H, and yield strength σ_y, can be expressed as $H=n\cdot\sigma_y$, where n depends on the work hardening ability of the materials [41]. According to the hardness and yield strength of NC FeCoNi from Refs. [42,43], the ratio of hardness to yield strength was calculated to be ~3.3. Thus, the yield strength of NC FeCoNi alloy was estimated to be ~1.75 GPa. These values are much higher than those of CG counterparts [44]. Generally, solid solution strengthening (σ_{SS}), GB strengthening (σ_{GB}), twin boundary (TB) strengthening (σ_{TB}) and dislocation strengthening (σ_{dis}) are considered to be the main strengthening mechanisms for solid solutions. Reducing the grain size into the nano-meter regime can induce substantial strengthening, which can be estimated by the classical Hall−Petch relationship:

$$\sigma_{GB}=K^{HP}d^{-1/2} \tag{6}$$

where K^{HP} is the Hall–Petch coefficient, and d is the average grain diameter. The K^{HP} was taken as 226 MPa·μm$^{0.5}$ [45], while d is 26 nm from statistical TEM analysis. Thus, σ_{GB} is calculated to be 1395 MPa for the NC FeCoNi alloy. This means that GB strengthening is the main strengthening mechanism for this alloy, as it contributes ~80% of the yield strength. It is also worth noting that, for HEAs/MEAs, the solid solution strengthening term σ_{SS} can be folded into the intrinsic strength (or lattice friction stress), where the latter represents some 'average' resistance offered by all the constituent atoms [45]. It was reported that the presence of SRO in HEAs/MEAs exacerbates lattice distortion, giving rise to such high intrinsic lattice friction stress [20]. In such a case, although the atomic radius, shear modulus and Burgers vector of Fe, Co and Ni are quite similar to each other, the intrinsic lattice friction stress of the FeCoNi alloy is still as high as 168 MPa [45]. Based on the GB strengthening and intrinsic strength, the collective contributions from the other strengthening defects, such as stacking faults, twin boundaries and dislocations, elevated the yield strength to ~ 1.75 GPa.

4.3 Influencing factors of tribological properties

4.3.1 Nanostructuring effects

The wear rate of the NC FeCoNi alloy is substantially lower than that of the CG one. Lower wear rates were also observed in many other NC metals and alloys [31,46]. Generally, the relationship between wear rate and hardness can be described by the well-known Archard equation [47]:

$$W=k\frac{P}{H} \tag{7}$$

where W is the wear rate, k is the prefactor relative to material, and P is the applied load. Refining the grains into the nano-meter regime can elevate the hardness many times, so it is not unexpected that the wear rate of the NC FeCoNi alloy can be effectively reduced. Another factor that should be taken into consideration is surface oxidation, which is another important influencing factor for the wear resistance. For our present case, as shown in Fig. 8, SEM−EDS examinations reveal that oxygen can be readily detected on most areas of the worn surfaces, expect for those delaminated craters for both the NC and CG FeCoNi alloys under all loading speeds. To provide further insights into the chemical state of Fe, Co and Ni, X-ray photoelectron spectroscopy (XPS) analysis of the worn surface of both the NC and the CG FeCoNi alloys was also conducted. The results confirm the existence of various oxides of Fe, Co and Ni (Fig. 9). These results agreed with the EDS results, illustrating the formation of oxide layers on the worn surfaces of both alloys. It is worth noting that the XPS spectra of the wear tracks on the NC alloy show stronger oxide peaks, suggesting more extensive oxidation than the CG alloy. This is mainly because the high density of GBs in the NC alloys can not only act as preferential nucleation sites for oxides but also prove high diffusion paths for oxygen [31]. As a result, the oxides are easier to form on the wear surface of the NC alloy than the CG alloy. The more oxides on the wear surface are, the better protective effects can be provided to prevent the alloy form contacting with the Al_2O_3 ball [48]. Thus, a lower wear rate can be expected as illustrated in Fig. 10. It can be seen that the wear rate decreased with the increase of amount of oxygen. Taken as a whole, nanostructuring on the one hand, significantly strengthens the alloy and on the other hand, facilitates the formation of protective oxidation layers, both of which contribute to the noticeably decreased wear rate of the NC FeCoNi alloy. Besides, according to calculated results by

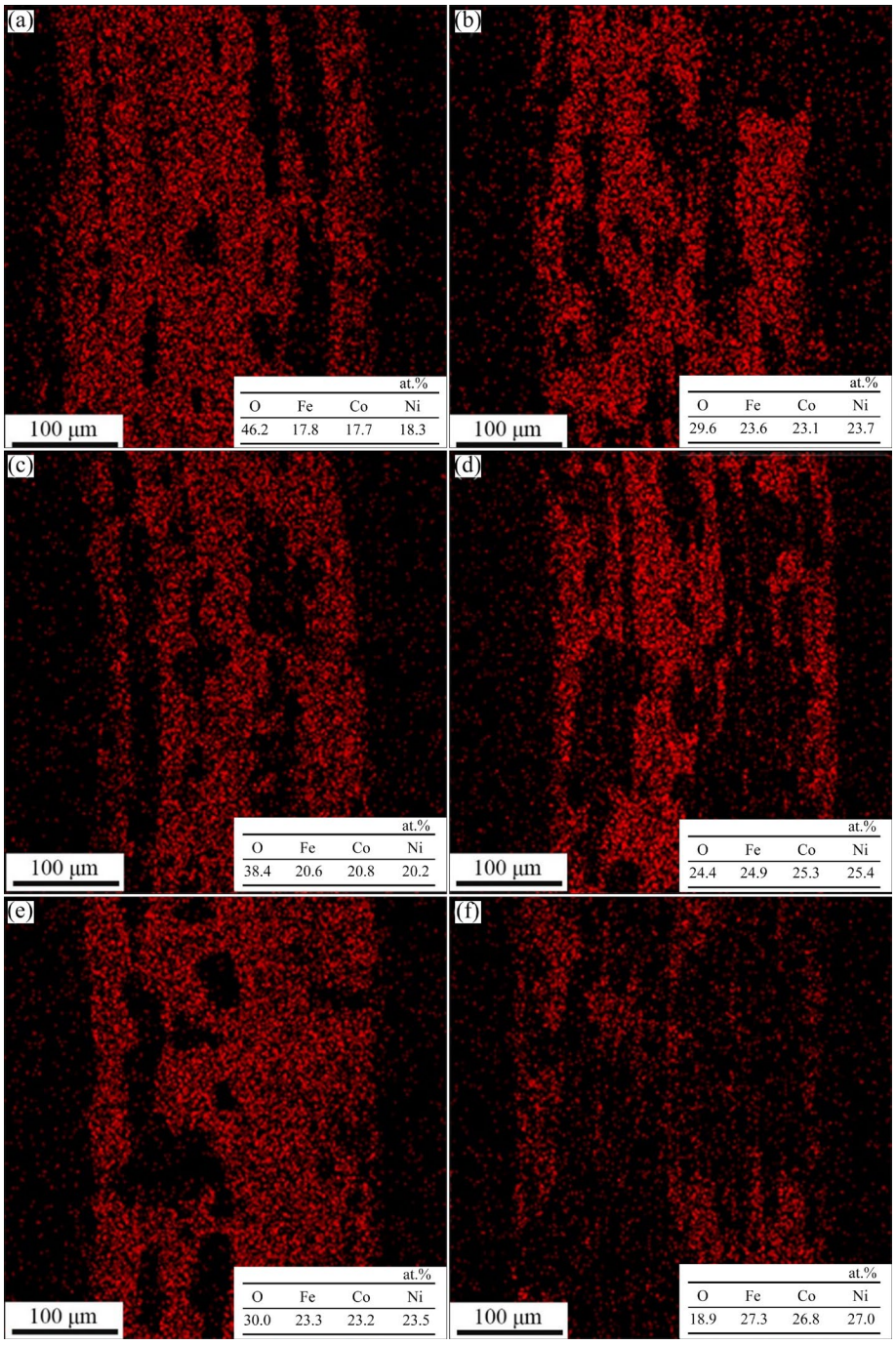

Fig. 8 Distribution of oxygen element on worn surfaces of NC (a, c, e) and CG (b, d, f) FeCoNi alloys at different sliding speeds: (a, b) 3.5 cm/s; (c, d) 5 cm/s; (e, f) 7 cm/s

Eqs. (4) and (5), the initial contact Hertzian stress induced plastic deformation in CG FeCoNi alloy. This is another reason for the high wear rate of CG FeCoNi alloy.

4.3.2 Compositional effects

We also compared the tribological properties of the present NC FeCoNi alloy with NC Ni and Ni-based dilute solid solutions in terms of COF and wear rate. All the data were collected from previous investigations under similar test conditions, as shown in Table 2. The NC FeCoNi alloy exhibits better wear resistance than these materials, as manifested by the lower COF and wear rate. The mean grain sizes of the NC metals and alloys listed in Table 2 are comparable, indicating that there are other factors that affect the wear resistance of the alloys beyond merely the grain refinement. In fact, it has been increasingly recognized that the fracture

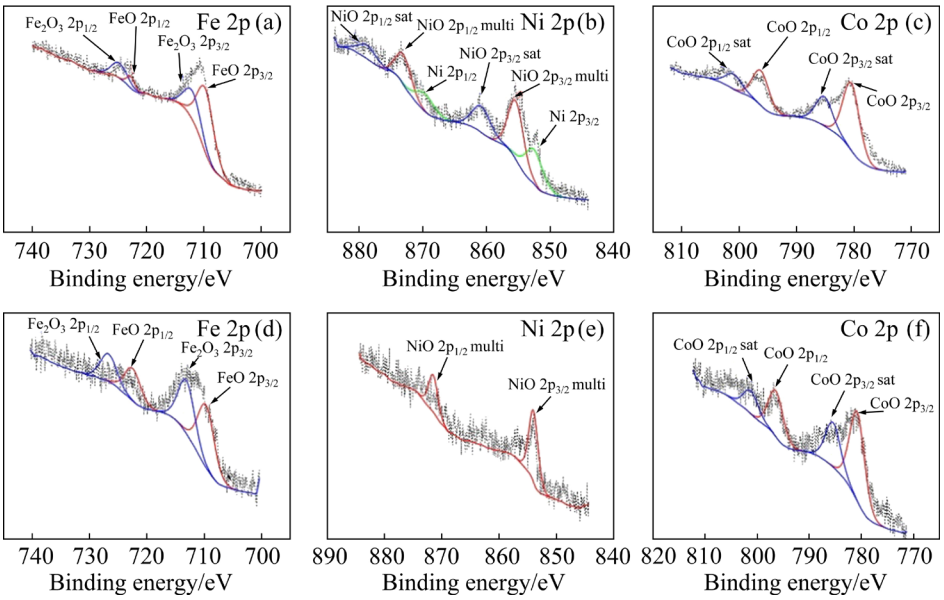

Fig. 9 XPS spectra obtained on worn surface of NC (a−c) and CG (d−f) FeCoNi alloys

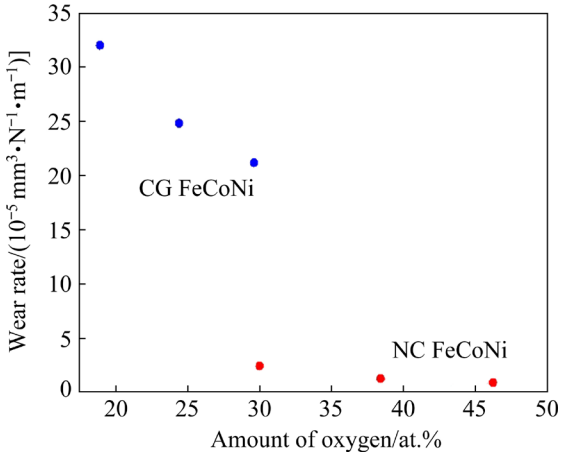

Fig. 10 Correlation between wear rate and oxidation for NC and CG FeCoNi alloys

Table 2 COF and wear rate of NC Ni and Ni-based binary alloys

Material	COF	Wear rate/ ($mm^3 \cdot N^{-1} \cdot m^{-1}$)
16 nm Ni [53]	0.62	6×10^{-4}
26 nm Ni [54]	0.6	1.2×10^{-4}
14 nm Ni−Fe [55]		1.92×10^{-4}
14 nm Ni−Fe [56]		7.9×10^{-4}
5−13 nm Ni−Mo [57]	0.6−0.8	2×10^{-4}–6.2×10^{-4}
13−17 nm Ni−Co [58]	0.62	5.9×10^{-4}

toughness is also a key factor affecting wear resistance, especially in abrasive, impact and erosive wear [49]. The fracture toughness of a given material is closely related to its strain hardening ability [50]. However, strain hardening is always absent in conventional NC metals and alloys, as dislocation can hardly be stored inside the tiny grains [51]. But for NC FeCoNi alloy, the interaction among concentrated constituent species intensifies lattice distortion and thus induces a high lattice friction stress. More than that, the SRO clusters at the atomic level, together with composition undulations that may be introduced on the nanometer scale during electrodeposition [52] rough the energy landscape of dislocation motion [35]. As a result, dislocations slip in a sluggish manner, which facilitates dislocation interlocks and accumulations within nano-grains, giving rise to enhanced strain hardening ability [52].

In fact, our nano-indentation tests do reveal that the NC FeCoNi alloy exhibits improved strain hardening ability. As shown in Fig. 11, after cube-corner indenter unloading, pile-ups around the indent impressions can be readily seen for the NC FeCoNi alloy, which means that the contact height (h_c) is higher that of the normal height (h). For work hardened metals, the strain hardening exponent (n) can be calculated by [59]

$$\sigma_r = \sigma_y \left(1 + \frac{E}{\sigma_y}\varepsilon_r\right)^n \tag{8}$$

where σ_y is the yield stress, E is the Young's modulus, σ_r is the stress corresponding to a representative strain ε_r, and ε_r is 0.126 for the cube-

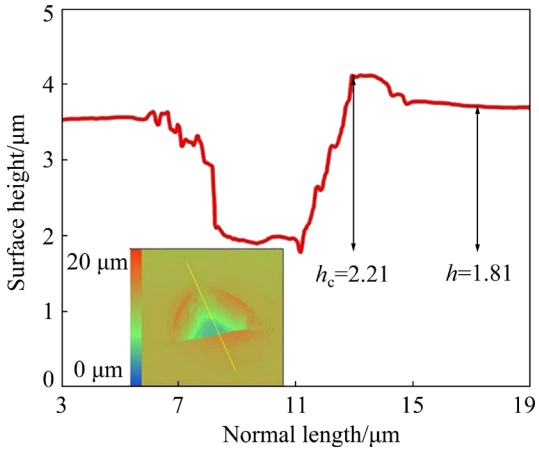

Fig. 11 Surface height profile around cube-corner indent for NC FeCoNi alloy (Inset: corresponding surface topography)

corner indenter. σ_y is calculated by $H/3.3$, and E is shown in Fig. 6. σ_r can be calculated by

$$\Pi_1 = C/\sigma_r \tag{9}$$

where Π_1 is a dimensionless function, C is the loading curvature. For the cube-corner indenter θ=42.3°, the expression of the two parameters can be described as

$$C=\pi H\left(\tan\theta\frac{h_c}{h}\right)^2 \tag{10}$$

$$\Pi_1 = 0.02842\left[\ln\left(\frac{E^*}{\sigma_r}\right)\right]^3 - 0.648\left[\ln\left(\frac{E^*}{\sigma_r}\right)\right]^2 + 4.9036\left[\ln\left(\frac{E^*}{\sigma_r}\right)\right] - 3.806 \tag{11}$$

where E^* is the reduced modulus and can be calculated as

$$E^* = 1/\left(\frac{1-\upsilon^2}{E}+\frac{1-\upsilon_i^2}{E_i}\right) \tag{12}$$

where E_i, υ_i and E, υ are the Young's modulus and Poisson's ratio of the diamond indenter and the specimen, respectively. The average value of h_c/h was calculated to be ~1.26 based on 25 indents. Thus, according to Eqs. (8)−(12), the strain hardening exponent (n) is calculated to be 0.22 for the NC FeCoNi alloy. This value is even higher than that obtained in the hierarchical nanostructured NiCo alloy, which exhibits excellent wear resistance [60]. Such enhanced strain hardening ability of NC FeCoNi can help to improve the wear resistance by suppressing local cracking and brittle delamination during abrasive wear. Base on above analysis, we can infer that it is the combined effects of nanostructuring and chemical complexity endow the NC FeCoNi alloy with ameliorated wear resistance.

5 Conclusions

(1) The activation volumes in the NC and CG FeCoNi alloy were calculated to be ~$7b^3$ and ~$24b^3$, respectively, both of which are much smaller than those in conventional FCC metals. Thermally activated deformation analysis reveal that the rate-controlling mechanisms in the NC FeCoNi alloy are the interaction of dislocations with GBs and nanoscale inhomogeneity such as SROs, while the latter is also the dominated activated process in the CG FeCoNi alloy.

(2) The hardness of the NC FeCoNi alloy was measured to be ~6.2 GPa, which is three times higher that of the CG counterpart (2 GPa). Such a high hardness is primarily attributed to GB strengthening, while solid-solution strengthening and TB strengthening also made some contributions.

(3) The main wear mechanism of the NC FeCoNi alloy is delamination wear, while both delamination wear and abrasive wear occur in the CG alloy. The NC FeCoNi alloy exhibits a significantly low wear rate, which is one order of magnitude lower than its CG counterpart. This was achieved by the synergetic effect of the significantly elevated hardness and the easy formation of the surface oxide layer, both of which are attributed to the substantially refined nano-sized grains.

(4) The NC FeCoNi alloy exhibits enhanced wear resistance compared with conventional NC Ni and Ni-based alloys, as manifested by the lowest wear rate and wear coefficient. This mainly stems from the improved strain hardening ability, owing to the extra resistance to dislocation motion imposed by the nanoscale inhomogeneity implicitly occurring in the MEAs.

CRediT authorship contribution statement

Yan CHEN: Resources, Investigation, Writing – Original draft; **Heng LI:** Conceptualization, Methodology; **Si-en LI:** Investigation; **Gui-xun SUN:** Methodology, Writing – Review & editing; **Liang ZHAO:** Visualization; **Chao-quan HU:** Resources,

Methodology; **Wei ZHANG:** Formal analysis, Writing – Review & editing; **Guo-dong TONG:** Formal analysis, Validation, Writing – Review & editing; **Xue-gang CHEN:** Resources, Validation; **Shuang HAN:** Conceptualization, Writing – Review & editing, Supervision, Project administration, Funding acquisition; **Hong-xiang ZONG:** Formal analysis, Funding acquisition; **Jun LI** and **Jian-she LIAN:** Supervision, Project administration.

Declaration of competing interest

The authors declare that they have no known competing financial interests or personal relationships that could have appeared to influence the work reported in this paper.

Acknowledgments

This work was supported by the Science and Technology Development Program of Jilin Province, China (No. 20160520007JH), the Major Science and Technology Special Project in Jilin Province, China (No. 20210301024GX), and the National Natural Science Foundation of China (Nos. 51601067, 51775266, 52301169).

References

[1] ZHANG Yong, ZUO T Ting-ting, TANG Zhi, GAO M C, DAHMEN K A, LIAW P K, LU Z P. Microstructures and properties of high-entropy alloys [J]. Progress in Materials Science, 2014, 61: 1−93.

[2] YEH J W, CHEN S K, LIN S J, GAN J Y, CHIN T S, SHUN T T, TSAU C H, CHANG S Y. Nanostructured high-entropy alloys with multiple principal elements: Novel alloy design concepts and outcomes [J]. Advanced Engineering Materials, 2004, 6: 299−303.

[3] GAO Peng, MA Zi-hao, GU Ji, NI Song, SUO Tao, LI Yu-long, SONG Min, MAI Y-W, LIAO Xiao-zhou. Exceptional high-strain-rate tensile mechanical properties in a CrCoNi medium-entropy alloy [J]. Science China Materials, 2022, 65: 811−819.

[4] SONG Hong-quan, TIAN Fu-yuan, WANG Dong-ping. Thermodynamic properties of refractory high entropy alloys [J]. Journal of Alloys and Compounds, 2016, 682: 773−777.

[5] YANG Mu-xin, YAN Ding-shun, YUAN Fu-ping, JIANG Ping, MA E, WU Xiao-lei. Dynamically reinforced heterogeneous grain structure prolongs ductility in a medium-entropy alloy with gigapascal yield strength [J]. Proceedings of the National Academy of Sciences of the United States of America, 2018, 115: 7224−7229.

[6] SU Jing, RAABE D, LI Zhi-ming. Hierarchical microstructure design to tune the mechanical behavior of an interstitial TRIP-TWIP high-entropy alloy [J]. Acta Materialia, 2019, 163: 40−54.

[7] GWALANI B, GORSSE S, CHOUDHURI D, ZHENG Yu-feng, MISHRA R S, BANERJEE R. Tensile yield strength of a single bulk Al0.3CoCrFeNi high entropy alloy can be tuned from 160 MPa to 1800 MPa [J]. Scripta Materialia, 2019, 162: 18−23.

[8] CAI Yun-peng, WANG Geng-jie, MA Yu-jie, CAO Zhen-hua, MENG Xiang-kang. High hardness dual-phase high entropy alloy thin films produced by interface alloying [J]. Scripta Materialia, 2019, 162: 281−285.

[9] GAO Peng, SUN Shuo, LI Heng, NIU R, HAN Shuang, ZONG Hong-xiang, WANG Hao, LIAN Jian-she, LIAO Xiao-zhou. Ultra-strong and thermally stable nanocrystalline CrCoNi alloy [J]. Journal of Materials Science & Technology, 2022, 106: 1−9.

[10] SUN Shuo, GAO Peng, SUN Gui-xun, CAI Ze-yu, HU Jiang-jiang, HAN Shuang, LIAN Jian-she, LIAO Xiao-zhou. Nanostructuring as a route to achieve ultra-strong high- and medium-entropy alloys with high creep resistance [J]. Journal of Alloys and Compounds, 2020, 830: 154656−154668.

[11] MA Yi, PENG Guang-jian, WEN Dong-hui, ZHANG Tai-hua. Nanoindentation creep behavior in a CoCrFeCuNi high-entropy alloy film with two different structure states [J]. Materials Science and Engineering A, 2015, 621: 111−117.

[12] JEHN H A. Multicomponent and multiphase hard coatings for tribological applications [J]. Surface and Coatings Technology, 2000, 131: 433−440.

[13] KIM Y S, PARK H J, MUN S C, JUMAEV E, HONG S H, SONG G, KIM J T, PARK Y K, KIM K S, JEONG S I, KWON Y H, KIM K B. Investigation of structure and mechanical properties of TiZrHfNiCuCo high entropy alloy thin films synthesized by magnetron sputtering [J]. Journal of Alloys and Compounds, 2019, 797: 834−841.

[14] RONG Zhi-yi, WANG Chao-hui, WANG You, DONG Meiling, YOU Yuan, WANG Jianing, LIU Hui-nan, LIU Jia-qi, WANG Yu-hang, ZHU Zhong-yu. Microstructure and properties of FeCoNiCrX (X=Mn, Al) high-entropy alloy coatings [J]. Journal of Alloys and Compounds, 2022, 921: 166061−166068.

[15] XIANG Kang, CHAI Lin-jiang, ZHANG Cheng-quan, GUAN Hao-tai, WANG Yue-yang, MA Yan-long, SUN Qi, LI Yu-qiong. Investigation of microstructure and wear resistance of laser-clad CoCrNiTi and CrFeNiTi medium-entropy alloy coatings on Ti sheet [J]. Optics & Laser Technology, 2022, 145: 107518−107526.

[16] CHAI Lin-jiang, WANG Chao, XIANG Kang, WANG Yue-yuan, WANG Tao, MA Yan-long. Phase constitution, microstructure and properties of pulsed laser-clad ternary CrNiTi medium-entropy alloy coating on pure titanium [J]. Surface and Coatings Technology, 2020, 402: 126503−126533.

[17] CAO Li-jun, HOU Chao, TANG Fa-wei, HAN Tie-long, HUANG Xin-tao, LI Yu-rong, WU Gao-chao, LIU Chao, LIANG Shu-hua, LUAN Jun-hua, JIAO Zeng-bao, NIE Zuo-ren, SONG Xiao-yan. Wear-resistance enhancement of nanostructured W−Cu−Cr composites [J]. International Journal of Refractory Metals and Hard Materials, 2021, 101: 105673−105682.

[18] YAN Xue, XU Jian-yan, GUAN Xiang-he, HAN Bing-yuan, ZHANG Cheng, CUI Zi-ruo, LIANG Wen-ping. Optimization of microstructure and properties of laser

sintered Ni30Cr25Al15Co15Mo5Ti5Y5 high-entropy alloy coatings via controlling plasma [J]. Transactions of Nonferrous Metals Society of China, 2023, 33: 168−188.

[19] MA E, WU X L. Tailoring heterogeneities in high-entropy alloys to promote strength-ductility synergy [J]. Nature Communications, 2019, 10: 5623−5632.

[20] ZHANG Ruo-peng, ZHAO Shi-teng, DING Jun, CHONG Yan, JIA Tao, OPHUS C, ASTA M, RITCHIE R O, MINOR A M. Short-range order and its impact on the CrCoNi medium-entropy alloy [J]. Nature, 2020, 581: 283−287.

[21] LEI Zhi-feng, LIU Xiong-jun, WU Yuan, WANG Hui, JIANG Sui-he, WANG Shu-dao, HUI Xi-dong, WU Yi-dong, GAULT B, KONTIS P, RAABE D, GU Lin, ZHANG Qing-hua, CHEN Hou-wen, WANG Hong-tao, LIU Jia-bin, AN K, ZENG Qiao-shi, NIEH T G, LU Zhao-pin. Enhanced strength and ductility in a high-entropy alloy via ordered oxygen complexes [J]. Nature, 2018, 563: 546−550.

[22] PENG Jian, LI Zi-you, JI Xin-bo, SUN Yan-le, FU Li-ming, SHAN Ai-dang. Decomposition kinetics of carbon-doped FeCoCrNiMn high-entropy alloy at intermediate temperature [J]. Transactions of Nonferrous Metals Society of China, 2020, 30: 1884−1894.

[23] LU Wen-jie, LUO Xian, YANG Yan-qin, HUANG Bin. Hall−Petch relationship and heterogeneous strength of CrCoNi medium-entropy alloy [J]. Materials Chemistry and Physics, 2020, 251: 123073−123079.

[24] YANG Tao, ZHAO Yi-lu, TONG Yang, JIAO Zeng-bao, WEI Jie, CAI Jin-xiong, HAN Xiao-dong, CHEN Da, HU A, KAI Ji-jun, LU Ke, LIU Yong, LIU C T. Multicomponent intermetallic nanoparticles and superb mechanical behaviors of complex alloys [J]. Science, 2018, 362: 933−937.

[25] BUDI S, MUHAB S, PURWANTO A, KURNIAWAN B, MANAF A. Effect of the electrodeposition potential on the magnetic properties of FeCoNi films [J]. Materials Science, 2019, 37: 389−394.

[26] XU Jing-cai, HONG Bo, PENG Xiao-ling, WANG Xin-qin, GE Hong-liang, HU Jun. Preparation and magnetic properties of gradient diameter FeCoNi alloys nanowires arrays [J]. Chemical Physics Letters, 2021, 767: 138368−138376.

[27] HACHÉ M J R, TAM J, ERB U, ZOU Y. Electrodeposited nanocrystalline medium-entropy alloys — An effective strategy of producing stronger and more stable nanomaterials [J]. Journal of Alloys and Compounds, 2022, 899: 163233−163249.

[28] EL-SHERIK A M, ERB U. Synthesis of bulk nanocrystalline nickel by pulsed electrodeposition [J]. Journal of Materials Science, 1995, 30: 5743−5749.

[29] TORABINEJAD V, ALIOFKHAZRAEI M, ASSAREH S, ALLAHYARZADEH M H, ROUHAGHDAM A S. Electrodeposition of Ni−Fe alloys, composites, and nano coatings—A review [J]. Journal of Alloys and Compounds, 2017, 691: 841−859.

[30] DU Li-ming, LAN Li-wei, ZHU Shi, YANG Hui-jun, SHI Xiao-hui, LIAW P K, QIAO Jun-wei. Effects of temperature on the tribological behavior of Al0.25CoCrFeNi high-entropy alloy [J]. Journal of Materials Science & Technology, 2019, 35: 917−925.

[31] SHAFIEI M, ALPAS A T. Effect of sliding speed on friction and wear behaviour of nanocrystalline nickel tested in an argon atmosphere [J]. Wear, 2008, 265: 429−438.

[32] DAO Ming, LU Lei, ASARO R J, de HOSSON J T M, MA E. Toward a quantitative understanding of mechanical behavior of nanocrystalline metals [J]. Acta Materialia, 2007, 55: 4041−4065.

[33] ZHU Yun-tian, HUANG Jian-yu, GUBICZA J, UNGÁR T, WANG Yin-min, MA E, VALIEV R Z. Nanostructures in Ti processed by severe plastic deformation [J]. Journal of Materials Research, 2003, 18: 1908−1917.

[34] DING Jun, YU Qin, ASTA M, RITCHIE R O. Tunable stacking fault energies by tailoring local chemical order in CrCoNi medium-entropy alloys [J]. Proceedings of the National Academy of Sciences of the United States of America, 2018, 115: 8919−8924.

[35] LI Qing-jie, SHENG H, MA E. Strengthening in multi-principal element alloys with local-chemical-order roughened dislocation pathways [J]. Nature Communications, 2019, 10: 3563−3572.

[36] HONG S I, MOON J, HONG S K, KIM H S. Thermally activated deformation and the rate controlling mechanism in CoCrFeMnNi high entropy alloy [J]. Materials Science and Engineering A, 2017, 682: 569−576.

[37] MOON J, HONG S I, BAE J W, JANG M J, YIM D, KIM H S. On the strain rate-dependent deformation mechanism of CoCrFeMnNi high-entropy alloy at liquid nitrogen temperature [J]. Materials Research Letters, 2017, 5: 472−477.

[38] WU Zheng-gang, GAO Yan-fei, BEI Hong-bin. Thermal activation mechanisms and Labusch-type strengthening analysis for a family of high-entropy and equiatomic solid-solution alloys [J]. Acta Materialia, 2016, 120: 108−119.

[39] CONRAD H. Grain size dependence of the plastic deformation kinetics in Cu [J]. Materials Science and Engineering A, 2003, 341: 216−228.

[40] LI Heng, LIANG Ya-qin, ZHAO Lei, HU Jiang-jiang, HAN Shuang, LIAN Jian-she. Mapping the strain-rate and grain-size dependence of deformation behaviors in nanocrystalline face-centered-cubic Ni and Ni-based alloys [J]. Journal of Alloys and Compounds, 2017, 709: 566−574.

[41] BROOKS I, LIN P, PALUMBO G, HIBBARD G D, ERB U. Analysis of hardness–tensile strength relationships for electroformed nanocrystalline materials [J]. Materials Science and Engineering A, 2008, 491: 412−419.

[42] YIN Fei, HU Shuang, XU Rong, XIANG Seng, HUA Lin, CHENG G J. Ultrastrong medium entropy alloy with simultaneous strength-ductility improvement via heterogeneous nanocrystalline structures [J]. Materials Science and Engineering A, 2021, 823: 141631−141641.

[43] WATANABE A, YAMAMOTO T, TAKIGAWA Y. Tensile strength of nanocrystalline FeCoNi medium-entropy alloy fabricated using electrodeposition [J]. Scientific Reports, 2022, 12: 12076−12083.

[44] WU Zheng-gang, BEI Hong-bin, PHARR G M, GEORGE E P. Temperature dependence of the mechanical properties of equiatomic solid solution alloys with face-centered cubic crystal structures [J]. Acta Materialia, 2014, 81: 428−441.

[45] ZHAO Yang-yang, NIEH T G. Correlation between lattice distortion and friction stress in Ni-based equiatomic alloys [J]. Intermetallics, 2017, 86: 45−50.

[46] CHAMANI M, FARRAHI G H, MOVAHHEDY M R.

Friction behavior of nanocrystalline nickel near the Hall−Petch breakdown [J]. Tribology International, 2017, 107: 18−24.
[47] RUPERT T J, SCHUH C A. Sliding wear of nanocrystalline Ni−W: Structural evolution and the apparent breakdown of Archard scaling [J]. Acta Materialia, 2010, 58: 4137−4148.
[48] VIÁFARA C C, CASTRO M I, VÉLEZ J M, TORO A. Unlubricated sliding wear of pearlitic and bainitic steels [J]. Wear, 2005, 259: 405−411.
[49] ZHOU Lian-yi, LIU Guo-zhong, HAN Zhong, LU Ke. Grain size effect on wear resistance of a nanostructured AISI52100 steel [J]. Scripta Materialia, 2008, 58: 445−448.
[50] XU Xiao-jun, XU Wei, EDERVEEN F H, van der ZWAAG S. Design of low hardness abrasion resistant steels [J]. Wear, 2013, 301: 89−93.
[51] OVID'KO I A, VALIEV R Z, ZHU Y T. Review on superior strength and enhanced ductility of metallic nanomaterials [J]. Progress in Materials Science, 2018, 94: 462−540.
[52] LI Heng, ZONG Hong-xiang, LI Su-zhi, JIN Shen-bao, CHEN Yan, CABRAL M J, CHEN Bing, HUANG Qqian-wei, CHEN Yan, REN Yang, YU Kai-yuan, HAN Shuang, DING Xiang-dong, SHA Gang, LIAN Jian-she, LIAO Xiao-zhou, MA E, SUN Jun. Uniting tensile ductility with ultrahigh strength via composition undulation [J]. Nature, 2022, 604: 273−279.
[53] WANG Li-pin, GAO Yan, XU Tao, XUE Qun-ji. A comparative study on the tribological behavior of nanocrystalline nickel and cobalt coatings correlated with grain size and phase structure [J]. Materials Chemistry and Physics, 2006, 99: 96−103.
[54] MA Guo-liang, YANG Jian-qun, LIU Yong, HE Shi-yu, JIANG Zhong-hao. Friction and wear behavior of nanocrystalline nickel in air and vacuum [J]. Tribology Letters, 2013, 49: 481−490.
[55] TORABINEJAD V, ALIOFKHAZRAEI M, ROUHAGHDAM A S, ALLAHYARZADEH M H. Tribological performance of Ni−Fe−Al_2O_3 multilayer coatings deposited by pulse electrodeposition [J]. Wear, 2017, 380/381: 115−125.
[56] TORABINEJAD V, ROUHAGHDAM A S, ALIOFKHAZRAEI M, ALLAHYARZADEH M H. Electrodeposition of Ni−Fe and Ni−Fe-(nano Al_2O_3) multilayer coatings [J]. Journal of Alloys and Compounds, 2016, 657: 526−536.
[57] LIU Jian-hong, LI Wen-hua, PEI Zhi-liang, GONG Jun, SUN Cao. Investigations on the structure and properties of nanocrystalline Ni−Mo alloy coatings [J]. Materials Characterization, 2020, 167: 110532−110543.
[58] WANG Li-ping, GAO Yan, XUE Qun-ji, LIU Hui-wen, XU Tao. Graded composition and structure in nanocrystalline Ni−Co alloys for decreasing internal stress and improving tribological properties [J]. Journal of Physics D: Applied Physics, 2005, 38: 1318−1324.
[59] BUCAILLE J L, STAUSS S, FELDER E, MICHLER J. Determination of plastic properties of metals by instrumented indentation using different sharp indenters [J]. Acta Materialia, 2003, 51: 1663−1678.
[60] CHEN Yan, CAI Ze-yu, LI Heng, SUN Gui-xun, ZHAO Liang, HAN Shuang, AN Jian, LIAN Jian-she. Optimizing mechanical and tribological properties of electrodeposited NiCo alloy coatings by tailoring hierarchical nanostructures [J]. Surface and Coatings Technology, 2022, 450: 129027−129037.

结构纳米化对 FeCoNi 中熵合金力学行为及摩擦磨损性能的影响

陈 岩[1]，李 恒[2]，李斯恩[1]，孙贵训[1]，赵 亮[1]，胡超权[1,3]，
张 炜[4]，佟国栋[4]，陈学罡[4]，韩 双[1]，宗洪祥[2]，李 军[4]，连建设[1]

1. 吉林大学 材料科学与工程学院 汽车材料教育部重点实验室，长春 130025；
2. 西安交通大学 金属材料强度国家重点实验室，西安 710049；
3. 吉林大学 超硬材料国家重点实验室，长春 130025；
4. 中国第一汽车股份有限公司，长春 130011

摘 要：通过纳米压痕测试和球盘摩擦实验，系统研究结构纳米化对 FeCoNi 中熵合金力学行为及干滑动摩擦磨损性能的影响。结果表明，将晶粒尺寸减小至纳米尺度，一方面显著提高了合金的硬度，另一方面促进了表面氧化层的形成。二者的共同作用使纳米晶 FeCoNi 合金的磨损率比粗晶合金低了一个数量级。与传统的纳米晶 Ni 及 Ni 基合金相比，纳米晶 FeCoNi 合金具有显著降低的磨损率和摩擦系数，表现出优异的耐磨性。这主要是由于纳米晶 FeCoNi 合金中本征的微尺度成分起伏能够有效阻碍位错滑移，使合金的应变硬化能力显著提高所致。

关键词：中熵合金；FeCoNi 合金；纳米晶；力学行为；干滑动磨损；成分起伏

(Edited by Xiang-qun LI)